Optimal Material Properties for Mitigating Brain Injury During Head Impact

Matthew R. Begley

Frank W. Zok

Materials Department,
University of California,
Santa Barbara, CA 93106

We present a methodology for identifying constitutive responses of crushable, linear-softening materials that would reduce the severity of brain injury caused by head impact in a typical automobile or sports collision. It is based on analysis of accelerations imparted to a spherical mass (representative of the human head) upon impact at prescribed velocity onto a flat padded structure. The resulting acceleration–time histories are used to calculate the corresponding Head Injury Criterion (HIC): a weighted product of acceleration and impact duration that has been found to correlate with the severity of brain injury. In the best-case scenario, the HIC is reduced by a factor of 1.84 relative to that obtained for a system optimized with a perfectly plastic foam. The optimal combinations of yield stress and crushing strain are not unique; that is, the optimum can be achieved with a range of strengths and crushing strains. The present solutions are expected to find utility in guiding the design of new polymer lattice materials for use in impact protection systems. [DOI: 10.1115/1.4024992]

1 Introduction

The severity of head impact in automobile collisions is characterized by the Head Injury Criterion (HIC) [1]. The HIC was first introduced by the U.S. National Highway Traffic Safety Administration for assessing risk of brain injury to vehicle occupants [2]. It was subsequently adopted for assessing the efficacy of protective equipment used for sporting applications [3,4] as well as the risk potential of surface materials used on playgrounds [5] and for cheerleading [6]. It is defined as [2,3]

$$\mathrm{HIC} = \max_{t_1,t_2}\left\{\left[\frac{\int_{t_1}^{t_2} a(t)dt}{t_2 - t_1}\right]^{5/2}(t_2 - t_1)\right\} \tag{1}$$

where a is acceleration in units of g (the acceleration due to gravity), t is time, and t_2 and t_1 are the two times that maximize the quantity in $\{\ldots\}$, subject to the constraint that the two times not differ from one another by more than a prescribed amount, t_c (typically 15 ms). The time restriction reflects the fact that low acceleration levels over extended periods of time pose low risk of injury.

In a previous study [7], we presented an analytical framework for identifying optimal properties of protective materials for mitigating brain injury during blunt head impact, assuming rigid, perfectly plastic material behavior up to densification. This was accomplished by analyzing the motion of a spherical mass (representing, roughly, a human head) as it impacts a foam pad mounted on a flat rigid structure (Fig. 1). Here we extend that analysis to include notional protective materials that exhibit *linear strain softening* after yield under compressive loading (Fig. 2). In principle, this behavior could be attained through the use of lattice materials that undergo buckling (either elastically or plastically) and, thus, exhibit a peak stress and subsequent softening in their compressive response [8].

The motivation for selecting this response stems from the observation that, for perfectly plastic foams, impact by a spherical mass produces an increasing acceleration with time (up to a peak) and, in turn, an HIC value that is considerably higher than that which could be obtained under conditions of constant acceleration. Here we show that, when optimized, strain softening materials exhibit a HIC that is 1.84 times lower than that obtained for an optimized system with a perfectly plastic foam.

The potential effects of these changes in HIC on probability of sustaining brain injuries with prescribed severity are shown in Fig. 3. For context, the limit set by the Federal Motor Vehicle Safety Standards for an adult head impacting the interior structure of an automobile at 6.7 m/s (15 mph) is 700 [2]. Accordingly, a reduction in HIC from 700 to 700/1.84 ≈ 400 would reduce the probability of serious nonlife-threatening head injury (3 on the Abbreviated Injury Scale) from 25% to 8% [9]. Proportional changes starting from higher baseline HICs would have even greater effect. For example, a reduction from 1300 to 700 would reduce the probability of the same head injury from 80% to 25%.

We restrict the scope of our analysis to impacts with initial velocities in the range of about 1–10 m/s and duration times in the range 1–30 ms. These encompass the majority of events associated with the secondary collision of an automobile occupant with the interior structure in typical automobile accidents. Moreover, this range is relevant to many common sports collisions. In this velocity–time domain, impact is essentially quasi-static in the sense that there is ample time for stress waves to travel over distances comparable to the dimensions of the human skull and, thus, a quasi-equilibrium state is attained.

The principal objective of the article is to identify constitutive responses of crushable materials that have potential for reducing the HIC relative to that obtained for a system optimized with perfectly-plastic foams. The analyses are similarly based on the impact of a spherical mass onto a crushable material mounted on a flat rigid support, as illustrated in Fig. 1. The constitutive responses are restricted to *rigid, linear-softening* materials that, upon densification, become rigid once again. In our previous work [7], we provide minimum velocities above which elasticity at very small strains can be neglected: the following assumes relevant design velocities are above this limit.

2 Impact Model

Let the target material response be denoted as $\sigma(\varepsilon, \varepsilon_c, \varepsilon_D)$, where ε is strain, ε_c is the crushing strain (i.e., that at which the flow stress drops to zero) and ε_D is the densification strain (Fig. 2). Provided $\varepsilon_C < \varepsilon_D$, the material supports no stress beyond the

Manuscript received May 31, 2013; final manuscript received June 25, 2013; accepted manuscript posted July 12, 2013; published online October 16, 2013. Editor: Yonggang Huang.

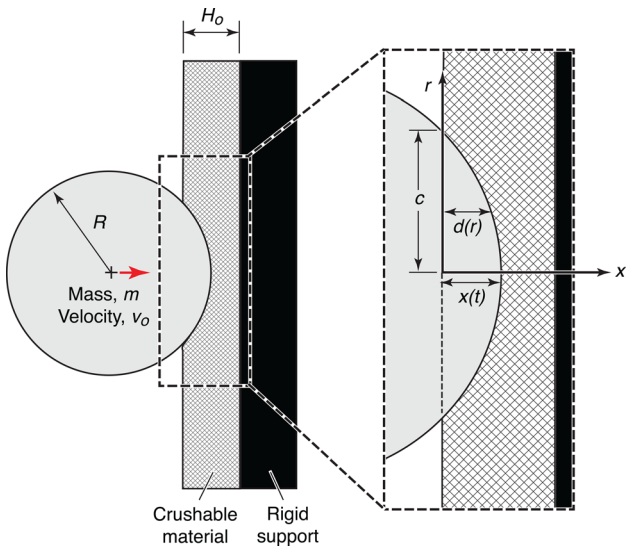

Fig. 1 Schematic of a spherical mass impacting a flat protective pad mounted on a flat rigid support

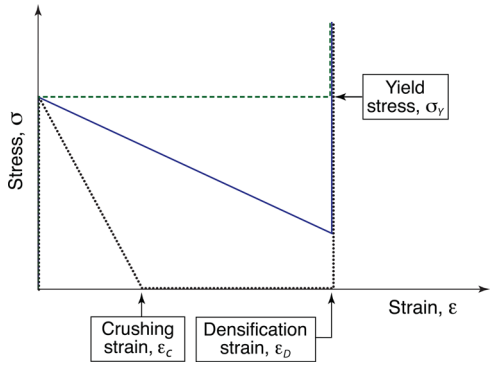

Fig. 2 Schematic of potential compressive stress–strain curves for protective materials

crushing strain, until densification, at which point the material stiffness rises dramatically and is treated as effectively rigid (dotted lines in Fig. 2). Otherwise, if $\varepsilon_C > \varepsilon_D$, the stress just before densification is finite and given by $\sigma_Y(1 - \varepsilon_D/\varepsilon_c)$ (solid lines). Further, the perfectly plastic limit (with no softening) occurs at $\varepsilon_C \to \infty$ (dashed lines). In this context, the crushing strain can be interpreted as the inverse of the slope of the softening response.

To solve the trajectory problem, it is convenient to express the target response in terms of displacement d (rather than strain), in which case $\sigma(d,\ d_c)$, where $d_c = \varepsilon_c H_o$. Densification is to be avoided, implying the constraint that $x_{\max} \leq \varepsilon_D H_o$, where $x_{\max}$ is the maximum penetration depth of the leading edge of the spherical mass. After solution, one can easily re-express the results in terms of ε_c and ε_D using these relationships. In what follows, the densification regime is not explicitly included in the material response; instead, it is accounted for by imposing the displacement constraint on the solution space.

For a spherical mass and scenarios where the penetration depth is much smaller than its radius, the penetration depth is given by

$$d(r,t) = x(t) - \frac{r^2}{2R} \tag{2}$$

where R is the sphere radius, $x(t)$ is the penetration depth of the leading edge, and t is time after impact. The penetration depth is zero at the contact radius $r = c$ implying that the contact radius is given by

$$c(t) = \sqrt{2Rx(t)} \tag{3}$$

Assuming a uniaxial response under the contact, the resistive force F acting against the sphere is given by

$$F[x(t)] = 2\pi \int_0^{\sqrt{2Rx(t)}} \sigma(d, d_c) r dr \tag{4}$$

For a rigid, perfectly plastic target (i.e., with $d_c \to \infty$), $\sigma(d) = \sigma_Y$, such that the net resistive force is

$$F(t) = \sigma_Y \pi c(t)^2 = 2\pi R \sigma_Y x(t) \tag{5}$$

Thus, we find that the response of a rigid-plastic target impacted by a sphere is identical to that of an elastic target with stiffness $k = 2\pi R\sigma_Y$.

For a linear softening material with finite d_c (i.e., nonzero slope to the stress–strain curve), the response of the target is given by

$$\sigma(d) = \sigma_Y \left(1 - \frac{d}{d_c}\right) \quad \text{for} \quad d < d_c \tag{6a}$$

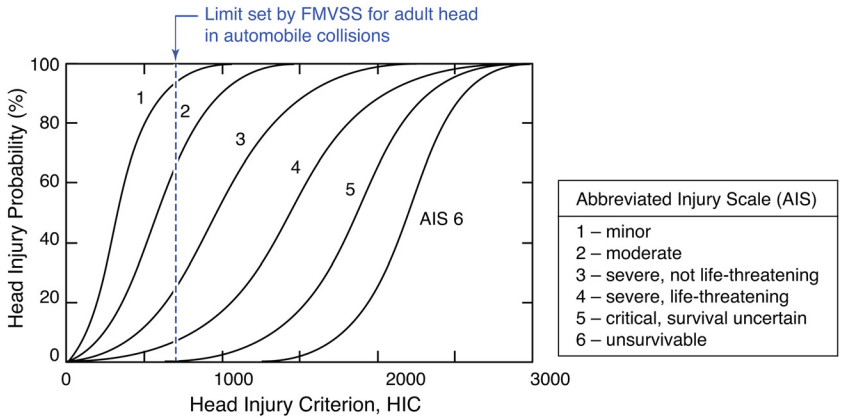

Fig. 3 Effects of HIC on probability of sustaining head injuries of varying severity (from 1 to 6 on the Abbreviated Injury Scale) and the current limit used by the Federal Motor Vehicle Safety Standards for adult vehicle occupants. The Abbreviated Injury Scale has been developed by the Association for the Advancement of Automotive Medicine. (Adapted from Refs. [2] and [8].)

$$\sigma(d) = 0 \quad \text{for} \quad d > d_c \tag{6b}$$

Reiterating, densification is avoided by imposing the constraint $x_{\max} \leq \varepsilon_D H_o$. The piecewise nature of the material response requires the contact force integral be broken into two segments: one associated with crushed material and another associated with the outer ring that is experiencing softening. Hence, the contact force is given by

$$F(t) = 2\pi \int_{r^*(t)}^{c(t)} \sigma_Y \left(1 - \frac{x(t) - \frac{r^2}{2R}}{d_c}\right) r dr \tag{7}$$

where $r^*(t) = \sqrt{2R(x(t) - d_c)}$ is the radius of the interior region of the contact that has fully crushed. This yields the contact force as a function of penetration distance $x(t)$

$$F(t) = 2\pi R \sigma_Y \begin{bmatrix} x(t)\left(1 - \frac{1}{2}\frac{x(t)}{d_c}\right) & \text{for} \quad x(t) < d_c \\ \frac{1}{2}d_c & \text{for} \quad x(t) > d_c \end{bmatrix} \tag{8}$$

Note that a linear-softening material with zero resistance past the critical penetration distance d_c still provides resistive force at all penetration depths. This is because the outer edges of the contact will always be in the nonzero region of the constitutive response and will, thus, provide finite resistive force. Moreover, once the leading edge of the sphere has passed the critical distance d_c, the resistive force (from Eq. (8)) is constant

$$F(t) = \pi R d_c \sigma_Y \tag{9}$$

In this limit, *the acceleration is constant*, provided densification is avoided. This is an important limit since, as we show below, it produces the minimum HIC.

The governing equation of motion for the sphere is determined simply by setting the resistive force of the target equal to the mass of the sphere times its acceleration. Let v_o be the initial (impact) velocity at the instant of contact, R be the characteristic length scale, and define the characteristic time as $t_o \equiv v_o/R$. With $\bar{x} \equiv x/R$, $\bar{d}_c \equiv d_c/R$ and $\tau \equiv t/t_o$, the governing equation in nondimensional form becomes

$$\overline{x'}(\tau) + \bar{\sigma}_Y \begin{bmatrix} \bar{x}(\tau)\left(1 - \frac{1}{2}\frac{\bar{x}(\tau)}{\bar{d}_c}\right) & \text{for} \quad \bar{x}(\tau) < \bar{d}_c \\ \frac{1}{2}\bar{d}_c & \text{for} \quad \bar{x}(\tau) > \bar{d}_c \end{bmatrix} = 0 \tag{10a}$$

$$\overline{x'}(0) = 1; \quad \bar{x}(0) = 0 \tag{10b}$$

where prime denotes differentiation with respect to τ (the normalized time) and the normalized yield stress is defined by

$$\bar{\sigma}_Y \equiv \frac{2\pi R^3 \sigma_Y}{m v_o^2} \tag{11}$$

This implies that the normalized response is only a function of the normalized crushing distance and the normalized yield stress, as in

$$\bar{x}(\tau) = f(\bar{d}_c, \bar{\sigma}_Y, \tau) \tag{12}$$

Again, note that the densification strain enters into the problem via the imposed constraint

$$\bar{x}_{\max} \equiv \frac{x_{\max}}{R} = \frac{\varepsilon_D H_o}{R} \tag{13}$$

Equation (10) can be trivially solved using conventional readily available time-stepping algorithms to yield the position–time function given as Eq. (12). From this, one can obtain the acceleration history of the sphere as it crushes the target and compute the HIC value.

The HIC computation in terms of normalized variables is written as

$$\text{HIC} = \left(\frac{v_o^2}{gR}\right)^{5/2} \left(\frac{R}{v_o}\right) \cdot \max \left[\left(\frac{\int_{t_1}^{\tau_2} -\overline{x''}(\tau) d\tau}{(\tau_2 - \tau_1)} \right)^{5/2} (\tau_2 - \tau_1) \right] \tag{14}$$

where the negative sign in front of $\overline{x''}(t)$ arises because the HIC definition uses the convention that deceleration has a positive sign. Note that the normalized acceleration–time response is only a function of $\bar{d}_c$ and $\bar{\sigma}_Y$. Hence, the general form of the HIC that accounts for all scaling possibilities is

$$\text{HIC} = \left(\frac{v_o^2}{gR}\right)^{5/2} \left(\frac{R}{v_o}\right) g(\bar{d}_c, \bar{\sigma}_Y) \tag{15}$$

where $g(\bar{d}_c, \bar{\sigma}_Y)$ is a dimensionless function that is invariant to changes in velocity, radius, and mass; thus, combinations of $\bar{d}_c$ and $\bar{\sigma}_Y$ that minimize g will also minimize the HIC. Naturally, the physical values of d_c and σ_Y that represent optimal solutions will change with velocity, radius, and mass according to Eq. (12) and the relation $d_c = R\bar{d}_c$. The key point is that once optimal combinations of $\bar{d}_c$ and $\bar{\sigma}_Y$ are known, optimal values of σ_Y and d_c can be computed for any set of impact parameters.

3 Optimal Material Properties

We first consider the case where $\bar{d}_c \to \infty$, which implies perfectly-plastic behavior. In this limit, a complete analytical solution is feasible: The motion of the spherical mass is described by

$$\bar{x}(\tau) = \frac{1}{\sqrt{\bar{\sigma}_Y}} \sin \sqrt{\bar{\sigma}_Y}\tau \tag{16a}$$

$$\tau_{\max} = \frac{\pi}{2\sqrt{\bar{\sigma}_Y}} \tag{16b}$$

$$\bar{x}_{\max} = \frac{1}{\sqrt{\bar{\sigma}_Y}} \tag{16c}$$

and the HIC is

$$\text{HIC} = \left(\frac{v_o^2}{gR}\right)^{5/2} \left(\frac{R}{v_o}\right) \cdot \max \left[(\cos \sqrt{\bar{\sigma}_Y}\tau_1)^{5/2} \left(\frac{\pi}{2\sqrt{\bar{\sigma}_Y}} - \tau_1\right)^{-3/2} \right] \tag{17}$$

One can readily show that the term in […] is maximized when $\tau_1 = 0.518/\sqrt{\bar{\sigma}_Y}$ and, thus, the HIC is given by

$$\text{HIC} = \left(\frac{v_o^2}{gR}\right)^{5/2} \left(\frac{R}{v_o}\right) \cdot 0.65(\bar{\sigma}_Y)^{3/4} \tag{18}$$

As expected, the HIC increases monotonically as the yield stress increases. Conversely, the maximum displacement increases monotonically as the yield stress *decreases* (Eq. (17)). Thus, the optimal solution is obtained at the constraint imposed by the maximum allowable displacement. Using the above normalizations, this implies

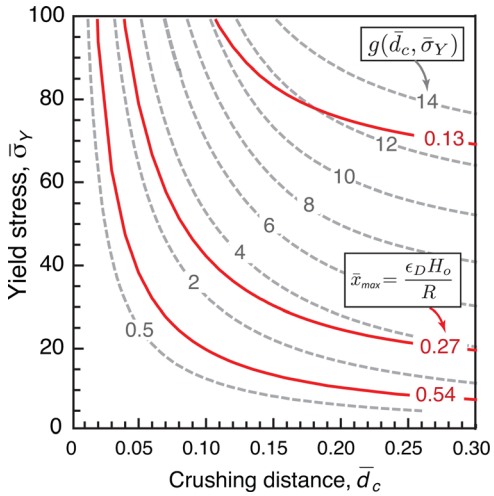

Fig. 4 Contours of normalized HIC, $g(\bar{d}_c, \bar{\sigma}_Y)$, as a function of $\bar{d}_c$ and $\bar{\sigma}_Y$, with contours of fixed stopping distance superimposed

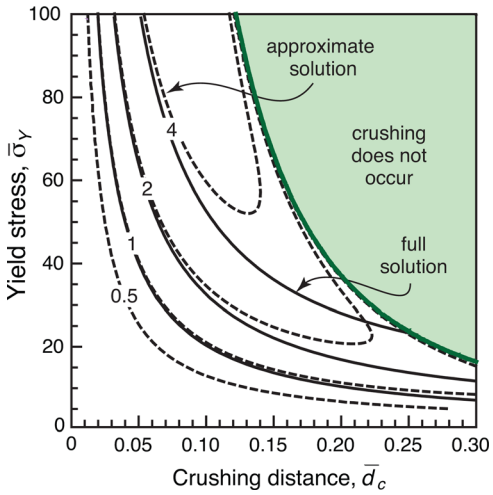

Fig. 5 HIC contours comparing the full solution (solid lines) with contours based on the approximate solution (dashed lines). The shaded space corresponds to combinations of target response for which the spherical mass arrests prior to crushing under its center. Note the approximation for $g(\bar{d}_c, \bar{\sigma}_Y)$ is inaccurate near this region. However, the predicted stopping distance is exact (i.e., not an approximation), and therefore, contours of equal stopping distance are identical to those shown in Fig. 4.

$$\bar{\sigma}_Y^{\text{opt}} = \frac{1}{\bar{x}_c^2}; \quad \sigma_Y^{\text{opt}} = \frac{mv_o^2}{2\pi R(\varepsilon_D H_o)^2} \tag{19}$$

$$\text{HIC}^{\text{opt}} = \left(\frac{v_o^2}{gR}\right)^{5/2}\left(\frac{R}{v_o}\right)\left(0.65\frac{1}{\bar{x}_c^{3/2}}\right) = 0.65\frac{v_o^4}{g^{5/2}(\varepsilon_D H_o)^{3/2}} \tag{20}$$

These results are identical to those reported in our previous study [7].

For linear-softening materials, the HIC as a function of $\bar{d}_c$ and $\bar{\sigma}_Y$ can be computed from the solution of Eqs. (10) and (14), yielding a form given by Eq. (15). In this regard, $g(\bar{d}_c, \bar{\sigma}_Y)$ represents a normalized HIC parameter that accounts for velocity and radius: mass factors in through the chosen value of $\bar{\sigma}_Y$. Similarly, we can compute $\bar{x}_{\max}(\bar{d}_c, \bar{\sigma}_Y)$. The optimal response is then given by minimizing g subject to the constraint on $\bar{x}_{\max}$.

Contours of $g(\bar{d}_c, \bar{\sigma}_Y)$ and $\bar{x}_{\max}(\bar{d}_c, \bar{\sigma}_Y)$ are shown in Fig. 4. Differences between linear-softening materials and perfectly plastic materials are best illustrated by a specific example. Consider a target with thickness $H_o = 40$ mm and $\varepsilon_D = 0.675$, and a sphere with $R = 100$ mm. The displacement constraint is $\bar{x}_{\max} = 0.27$ —the middle red contour shown in the figure. The minimum HIC achievable with a perfectly plastic material is $g_{pp} = 4.63$, obtained with $\bar{\sigma}_Y = 13.3$. (Note that this corresponds to the asymptote of the contour $g(\infty, \bar{\sigma}_Y) = 4.63$ and is calculated directly from Eqs. (18) and (19).) A softening material with $\bar{d}_c = 0.0527$ and $\bar{\sigma}_Y = 75$ can achieve $g_s = 2.71$; this corresponds to a crushing distance of 5.27 mm, or a crushing strain of $\varepsilon_C = 0.13$. The required initial yield stress for the softening material is about six times that of the optimal perfectly plastic material.

Note also that one obtains nearly equivalent results for g_s (0.04, 100) = 2.71, which corresponds to a slightly smaller crushing strain and slightly larger initial yield stress than the values cited above, but the same HIC value. Indeed, for small crushing distances, there are multiple combinations of initial yield stress and crushing strains that yield equivalent, near-optimal HIC values.

4 Discussion

In the limit that crushing strains are much smaller than the densification strain (i.e., $\varepsilon_C << \varepsilon_D$), an approximate analytical solution can be developed that clarifies the optimization problem. This scenario corresponds to cases where $\bar{d}_c << \bar{x}_{\max}$, i.e., the crushing distances are small in comparison to the stopping constraint. After crushing of the target directly under the sphere, the relevant dynamic solution is given by

$$\overline{x''}(\Delta\tau) = -\frac{\bar{d}_c\bar{\sigma}_Y}{2} \tag{21a}$$

$$\overline{x'}(\Delta\tau) = -\frac{\bar{d}_c\bar{\sigma}_Y}{2}\Delta\tau + \bar{v}_1 \tag{21b}$$

$$\bar{x}(\Delta\tau) = -\frac{\bar{d}_c\bar{\sigma}_Y}{4}\Delta\tau^2 + \bar{v}_1\Delta\tau + \bar{d}_c \tag{21c}$$

where $\Delta\tau$ is the time measured from the instant that $\bar{x} = \bar{d}_c$, i.e., $\Delta\tau = \tau - \tau_c$ where τ_c is the time associated with the crushing phase; and $\bar{v}_1$ is the normalized velocity at the end of the crushing phase (at the instant that $\bar{x} = \bar{d}_c$).

Equating the loss in kinetic energy of the spherical mass to the work done in crushing the target to $\bar{x} = \bar{d}_c$ yields the velocity $\bar{v}_1$

$$\frac{1}{2}m(v_o^2 - v_1^2) = \int_0^{d_c} F(x)dx = \frac{2Rd_c^2\sigma_Y}{3} \rightarrow \bar{v}_1 = \sqrt{1 - \frac{2}{3}\bar{d}_c^2\bar{\sigma}_Y} \tag{22}$$

This yields the solutions

$$\Delta\tau_{\max} = \frac{2\sqrt{1 - \frac{2\bar{d}_c^2\bar{\sigma}_Y}{3}}}{\bar{d}_c\bar{\sigma}_Y} \tag{23a}$$

$$\bar{x}_{\max} = \frac{\bar{d}_c}{3} + \frac{1}{\bar{d}_c\bar{\sigma}_Y} \tag{23b}$$

The displacement result is exact for scenarios where $\bar{d}_c^2\bar{\sigma}_Y < 3/2$ since this implies that the velocity after crushing is nonzero. Since the displacement at the end of the crushing phase is known (i.e., it is $\bar{d}_c$), the time associated with the crushing phase is not required.

The approximate HIC solution requires the assumption that the time associated with the crushing phase is small in comparison to the time needed to stop the object after this phase, i.e., $\Delta\tau >> \tau_c$, then $\Delta\tau_{\max} \approx \tau_{\max}$: assuming $\tau_1 \approx 0$ and $\tau_2 \approx \Delta\tau_{\max}$. The HIC in the limit of small crushing strains (relative to densification strain) is then

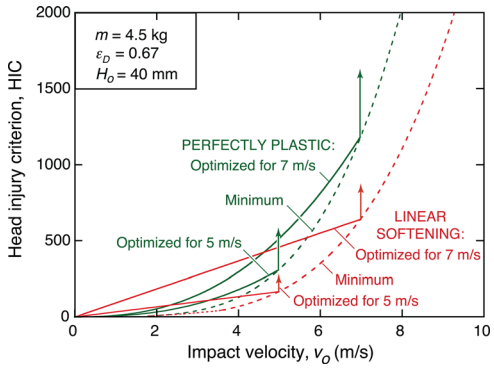

Fig. 6 HIC values for linear-softening and perfectly plastic materials optimized for two specific impact velocities (5 m/s and 7 m/s). Each dashed line represents the locus of minimum HIC values.

$$\mathrm{HIC} = \left(\frac{v_o^2}{gR}\right)^{5/2}\left(\frac{R}{v_o}\right)\left(\frac{(\bar{d}_c\bar{\sigma}_Y)^{3/2}}{2\sqrt{2}}\left[\sqrt{1-\frac{2\bar{d}_c^2\sigma_Y}{3}}\right]\right) \tag{24}$$

In the limit of small crushing distances relative to the sphere radius (i.e., $\bar{d}_c \ll 1$) these results further simplify to

$$\bar{x}_{\max} = \frac{1}{\bar{d}_c\bar{\sigma}_Y}$$
$$\mathrm{HIC} = \left(\frac{v_o^2}{gR}\right)^{5/2}\left(\frac{R}{v_o}\right)\frac{(\bar{d}_c\bar{\sigma}_Y)^{3/2}}{2\sqrt{2}} = \left(\frac{v_o^2}{gR}\right)^{5/2}\left(\frac{R}{v_o}\right)\frac{1}{2\sqrt{2}\bar{x}_{\max}^{3/2}} \tag{25}$$

The latter result is 1.84 times smaller than that for the perfect-plasticity material when impacted by a spherical mass. Additionally, it is identical to the result for *impact of a flat-ended cylindrical mass onto an optimized perfectly plastic foam (with constant contact area)*, wherein the acceleration is also constant for the duration of impact [7]. The implication is that responses of crushable materials that lead to constant acceleration are ones that minimize the HIC.

Typical results for the HIC values of optimized systems with perfectly plastic and linear-softening materials are presented in Fig. 6. Here we have considered systems optimized for impact velocities of either 5 m/s or 7 m/s for a foam thickness of 40 mm. The dashed lines represent the minimum possible HIC for each of the two constitutive responses and the solid lines represent the performance of the same systems optimized for the specified velocities.

It should be noted that, once optimized for a given impact velocity, the system becomes suboptimal for lower velocities. (At higher velocities, protection is lost because of the rapid hardening associated with densification.) For some applications, the performance of an optimized system over a range of velocities (including those below the velocity used for optimization) may become an important consideration in the design. Figure 6 shows that, whereas the performance of the system optimized with the linear-softening material is superior *slightly below* the velocity used for optimization, its performance becomes inferior to that of the system optimized for a perfectly plastic material at the same velocity once the velocity drops below a critical value.

5 Conclusions

We have presented a methodology for identifying constitutive responses of crushable linear-softening materials that have potential for reducing the HIC for impact of a spherical mass, relative to that obtained for a comparable system optimized with perfectly plastic foams. In the best-case scenario, the acceleration is essentially constant over the duration of impact and the HIC is reduced by a factor of 1.84. The same result has been previously obtained for a system optimized for 1D impact onto a perfectly plastic material. The property combinations that yield near-optimal behavior are not unique; they include a range of combinations of yield stress and crushing distance. Once optimized for one velocity, the HIC for lower velocities is higher than the minimum attainable value at the lower velocity. Furthermore, at sufficiently low impact velocities, a system optimized with a linear-softening material eventually becomes inferior (at low velocities) to that optimized with a perfectly plastic material. The implication is that compromise will likely play a role in the design of systems expected to provide protection over a range of impact velocities.

Finally, we note that, while the HIC provides a simple basis to evaluate the role of the target material (as done here), it provides little (if any) insight into the forces and deflections transmitted through the skull to the brain itself. Clearly, more work is needed to identify impact metrics that make explicit connections between: (1) the temporal and spatial details of contact pressure between the skull and target, (2) the temporal and spatial details of pressures transmitted from the skull to the brain, and (3) physically based predictors of various damage mechanisms in the brain.

Acknowledgment

This work was supported by the Institute for Collaborative Biotechnologies through grant W911NF-09-0001 from the U.S. Army Research Office.

References

[1] Gurdjian, E. S., Roberts, V. L., and Thomas, L. M., 1966, "Tolerance Curves of Acceleration and Intracranial Pressure Protective Index in Experimental Head Injury," J. Trauma, **6**, pp. 600–604.
[2] U.S. Department of Transportation, 1998, "Federal Motor Vehicle Safety Standards, Standard 208," http://www.nhtsa.gov/cars/rules/import/fmvss/#SN208
[3] Greenwald, R. M., Gwin, J. T., Chu, J. J., and J. J. Crisco, 2008, "Head Impact Severity Measures for Evaluating Mild Traumatic Brain Injury Risk Exposure," Neurosurgery, **62**, pp. 789–798.
[4] Naunheim, R. S., Standeven, J., Richter, C., and Lewis, L. M., 2000, "Comparison of Impact Data in Hockey, Football, and Soccer," J. Trauma Inj. Infect. Crit. Care, **48**, pp. 938–941.
[5] Lewis, L. M., Naunheim, R., Standeven, J., and Naunheim, K. S., 1993, "Quantitation of Impact Attenuation of Different Playground Surfaces Under Various Environmental Conditions Using a Tri-Axial Accelerometer," J. Trauma, **35**, pp. 932–935.
[6] Shields, B., and Smith, G. A., 2009, "The Potential for Brain Injury on Selected Surfaces Used by Cheerleaders," J. Athletic Train., **44**, pp. 595–602.
[7] Zok, F. W., Nazarian, O., and Begley, M. R., "Selecting Protective Materials for Mitigating Brain Injury During Blunt Impact," Int. J. Impact Eng. (submitted).
[8] Rinaldi, R. G., Bernal-Ostos, J., Hammetter, C. I., Jacobsen, A. J., and Zok, F. W., 2012, "Effects of Material Heterogeneities on the Compressive Response of Thiolene Pyramidal Lattices," J. Mater. Sci., **47**, pp. 6621–6632.
[9] Mackay, M., 2007, "The Increasing Importance of the Biomechanics of Impact Trauma," Sadhana, **32**, pp. 397–408.